

定量仿真研究贵金属纳米探针聚集诱导的非线性增强光热效应

张奇睿^{1,2}, 石玉娇^{1,2*}

¹华南师范大学生物光子学研究院, 激光生命科学教育部重点实验室, 广东 广州 510631;

²华南师范大学生物光子学研究院, 广东省激光生命科学重点实验室, 广东 广州 510631

摘要 贵金属纳米探针及其聚合物以优异的光热转换效率、良好的生物相容性及灵活可调的光学吸收峰位受到了光热治疗领域研究人员的广泛关注。本文通过有限元仿真定量演示了贵金属纳米探针聚集诱导的非线性光学及光热效应,系统地讨论了纳米颗粒的材质、尺寸、排列方式、聚集程度等因素对纳米探针光热转换效率的影响,并对局域表面等离子体共振耦合效应产生的非线性光场以及光热增强效应及其机制进行了深入定量分析。

关键词 生物光学; 纳米探针; 光热转换; 局域表面等离子体共振; 耦合效应

中图分类号 O439 文献标志码 A

DOI: 10.3788/CJL221254

1 引言

光热疗法是一种将光能转变为热能,通过局部加热并触发生化过程来杀死肿瘤细胞的肿瘤治疗方法^[1]。寻找一种光热转换效率高且具有足够安全性、靶向性的探针,是光热疗法开展的基础。同时,这样的探针也可作为光热源用于热声、光声成像等研究领域^[2-4],甚至可被用于多模态成像治疗一体化研究^[5]。在过去的几十年间,尺寸小于光波长的金属纳米颗粒已被广泛应用于光伏发电、光学传感和生物医学等领域^[6-12],这是由于其在外部光照射下可以产生局域表面等离子体共振。在尺寸适当的纳米颗粒中,受限的自由电子以与入射光波相同的频率振荡,并最终进入共振,产生强烈的、高度局域化的电磁场^[13],因而可观察到明显的消光现象。纳米颗粒吸收的光能可以通过非辐射损耗转化为热。由于局域表面等离子体共振强烈地依赖于具体的纳米结构,因此,调整消光峰的位置使之处于生物组织的光学窗口,或者调节消光强度使其具有合适的光热转换效率,理论上都可以通过对纳米探针进行形态学设计实现。由于调节孤立的单个纳米粒子与激发光的相互作用以及进一步改善其光学和热学性能的能力有限,因此,由多个纳米粒子聚集或自组装而成的纳米探针成为了研究热点^[14-15]。当颗粒间的距离小于或等于纳米颗粒的尺寸时,颗粒间复杂的相互作用会引起等离子体激元耦合^[16],使纳米探针表现出

丰富多样的新颖的非线性效应,进而使其在光学和热响应方面与它们的个体完全不同,因而具有更大的生物应用潜力。因此,基于局域表面等离子体共振耦合的贵金属纳米探针是新一代光热转换剂的热点研究和方向之一。

尽管相关研究已经证明了金纳米囊泡^[17]、纳米多触手^[18]、纳米枝状壳层^[19]、纳米团簇^[20]等纳米聚合体的实验应用,但目前仍缺乏相关定量研究。定量分析纳米颗粒聚集程度和形态对光热效率的影响,最大化获取纳米组件的耦合效应以提高操纵其光学性能和相应热学性能的能力,对于更加合理、有指导性地设计、构建和优化高效的等离子体纳米探针具有重要意义。本课题组利用有限元仿真定量演示了贵金属纳米探针聚集诱导的非线性光学及光热效应,获得了定量的温度场分布。进一步,本文基于纳米粒子的材质、尺寸、排列方式等探讨了纳米探针的光热转换效率,同时对局域表面等离子体共振耦合效应产生的非线性光场、光热增强效应及其机制进行了深入定量分析,以期设计更高效的等离子体纳米聚集探针提供系统和较为全面的理论指导。

2 基本原理与实验仿真

贵金属纳米探针的基于局域表面等离子体共振原理的强烈的光吸收,以及后续由无辐射跃迁热能释放引起的热过程,在生物学和生物医学领域有着广泛应

收稿日期: 2022-09-18; 修回日期: 2022-10-24; 录用日期: 2022-11-02; 网络首发日期: 2022-11-15

基金项目: 国家自然科学基金青年科学基金(61805085)、2017年度博士后创新人才支持计划(BX201700084)、中国博士后科学基金面上项目(2018M630961)

通信作者: *shiyuj@scnu.edu.cn

用和重要意义。照射探针的高强度激光与贵金属纳米探针之间的相互作用涉及多个时空尺度的物理过程,其中严格的理论分析需要包含量子连续能级理论的多尺度分析。为了简化问题,本文认为连续能级理论可以用于研究贵金属纳米探针的光吸收以及之后的热过程。

贵金属纳米探针的光吸收来源于孤立的单个纳米粒子的表面等离子体共振吸收以及纳米探针聚集引起的极强的粒子间耦合效应。后者是非线性光热增强效应的来源。当几何尺寸远小于光波长的纳米探针被强烈的激光照射时,纳米探针的电子云概率场会受到电磁场的扰动,从而偏离原先的平衡位置,发生来回振荡。假设贵金属纳米探针被一束激光照射(暂不考虑磁场的影响),该光可认为是频率为 ω 、电场强度为 \mathbf{E} 的时变电场,电场各分量以同样的角频率随时间呈时谐变化。该电场满足亥姆霍兹方程,即

$$\nabla \times (\mu_r^{-1} \nabla \times \mathbf{E}) - k_0^2 \left(\epsilon_r - i \frac{\sigma}{\omega \epsilon_0} \right) \mathbf{E} = 0, \quad (1)$$

式中: μ_r 为相对磁导率; ϵ_r 为相对介电常量; σ 为电导率; k_0 为角波数。单个纳米颗粒受到电场影响后,可将电子云偏离原先平衡位置的状态描述为一个电偶极子,则贵金属纳米探针中单个纳米颗粒之间的强粒子间耦合作用理论上可用耦合偶极子方程^[21]描述为

$$\mathbf{P}_j = \alpha_j \mathbf{E}_j = \alpha_j \left(\mathbf{E}_{\text{inc},j} - \sum_{k \neq j} \mathbf{A}_{jk} \mathbf{P}_k \right), \quad (2)$$

式中: \mathbf{P}_j 表示位于位置 \mathbf{r}_j 上的电偶极子的偶极矩; α_j 表示偶极子的极化率; \mathbf{E}_j 为该位置的电场强度,它是入射光波的外电场,同时也是入射电场 $\mathbf{E}_{\text{inc},j} = \mathbf{E}_0 \exp(i\mathbf{k}_0 \cdot \mathbf{r}_j - i\omega t)$ 及其所引起的附近所有其他偶极子所激发的电场的叠加(其中 \mathbf{E}_0 为入射电场的电场强度, \mathbf{k}_0 为入射光的波矢); \mathbf{P}_k 表示位于位置 \mathbf{r}_k 上的电偶极子的偶极矩。 \mathbf{A}_{jk} ($j \neq k$)可以写成一个三维矩阵,即

$$\mathbf{A}_{jk} = \frac{\exp(i\mathbf{k}_0 \cdot \mathbf{r}_{jk})}{r_{jk}} \times \left[k_0^2 (\hat{\mathbf{r}}_{jk} \hat{\mathbf{r}}_{jk} - \mathbf{M}_3) + \frac{ik_0 r_{jk} - 1}{r_{jk}^2} (3\hat{\mathbf{r}}_{jk} \hat{\mathbf{r}}_{jk} - \mathbf{M}_3) \right], \quad (3)$$

式中: $r_{jk} = |\mathbf{r}_j - \mathbf{r}_k|$; $\hat{\mathbf{r}}_{jk} = (\mathbf{r}_j - \mathbf{r}_k)/r_{jk}$; \mathbf{M}_3 为一个 3×3 的单位矩阵; k_0 为波矢的大小。定义 $\mathbf{A}_{jk} \equiv \alpha_j^{-1}$,则这个系统可以描述成一个复线性耦合偶极方程组,即

$$\sum_{k=1}^N \mathbf{A}_{jk} \mathbf{P}_k = \mathbf{E}_{\text{inc},j}, \quad (4)$$

式中: N 为系统中的偶极子总数。求解耦合偶极方程组后,纳米粒子间耦合的贵金属纳米探针的吸收截面^[22]可以表示为

$$C_{\text{abs}} = \frac{4\pi k_0}{|\mathbf{E}_0|^2} \sum_{j=1}^N \left\{ \text{Im} \left[\mathbf{P}_j \times (\alpha_j^{-1})^* \mathbf{P}_j^* \right] - \frac{2}{3} k_0^3 |\mathbf{P}_j|^2 \right\}. \quad (5)$$

电偶极子之间的相互作用非常复杂,很难得到解析

解。本文将基于有限元的计算方法作为定量技术,研究以局域表面等离子体共振为媒介的电场耦合和光吸收增强。为了系统地理解每个孤立纳米颗粒之间的共振耦合及其对光吸收的贡献,本文研究了三种基本耦合纳米结构,即孤立金纳米球、正三角形金纳米球三聚体和密排六边形金纳米球七聚体。单个金纳米球的直径(D)设置为15 nm,粒子间距离(d)设置为1 nm。入射激光平行于由箭头指示的轴偏振方向,如图1(a)~(c)所示。与孤立的纳米球相比,入射电磁辐射与耦合纳米结构的相互作用导致自由电子发生强极化和偶极振荡。当粒子间距离远小于纳米颗粒直径时,倏逝场引起的近场相互作用是主要的耦合机制。金纳米球的聚集程度越高,单个球体之间的耦合效应就越强烈。在本文仿真的三种结构中,金纳米球七聚体显示出最高的局域表面等离子体共振耦合效应和电场增强。电偶极子的集体共振会将电磁能量转换为热,产生的热功率密度可以通过电阻加热公式进行定量计算,计算公式为

$$Q_{\text{abs}} = \mathbf{J} \cdot \mathbf{E}, \quad (6)$$

式中: \mathbf{J} 是由自由电子振荡产生的电流密度。在模拟仿真中,将纳米探针设置为浸入在水中。采用电场强度的大小为 $E_0 = 4 \times 10^5$ V/m的平面电波照射探针,并通过有限元分析方法定量计算探针的光吸收。根据辐照度表达式 $I_{\text{inc}} = c \epsilon_0 n_{\text{sur}} E_0^2 / 2$ (其中 c 为光速, ϵ_0 为真空介电常数, n_{sur} 为周围环境的折射率),入射激光功率约为11.3 mW/ μm^2 。

图1(d)显示了孤立金纳米球、正三角形金纳米球三聚体和密排六边形金纳米球七聚体探针的光热功率谱仿真结果,其中最高吸收波长定义为局域表面等离子体共振波长。由图1(d)可以发现:随着纳米球聚集数量的增加,由于纳米球间的共振耦合增强,纳米探针的光热功率峰值非线性增大;同时,空间几何尺寸的增大使得局域表面等离子体共振峰红移。图1(e)清晰地显示出共振耦合的增强使得单个球体所贡献的光吸收大大增加,其中,七聚体中的每个纳米球的光热功率是孤立纳米球的2倍以上。这一结果表明,通过增加纳米球的聚集数量,利用粒子间的局域表面等离子体共振耦合可以大大提高每个粒子的光热转换效率。

纳米探针将吸收的激光能量转换为热,纳米探针成为热源,导致局部升温以及以其为中心的热扩散,温度场可以通过热扩散方程来描述,即

$$\rho C_p \frac{\partial T}{\partial t} = k \nabla^2 T + Q_{\text{abs}}, \quad (7)$$

式中: ρ 为密度; C_p 为比热容; T 为温度; k 为热导率。

为了进一步证明纳米探针的非线性增强光热效应,本文分别定量模拟了经激光照射一定时间后上述三种探针及其周围环境的温度场。在仿真中,设置纳米探针与周围环境的初始温度均为297.1 K,纳米探针在电场强度为 4×10^5 V/m的激光下照射10 ns。

图2(a)~(c)分别展示了经激光照射10 ns后,孤立金

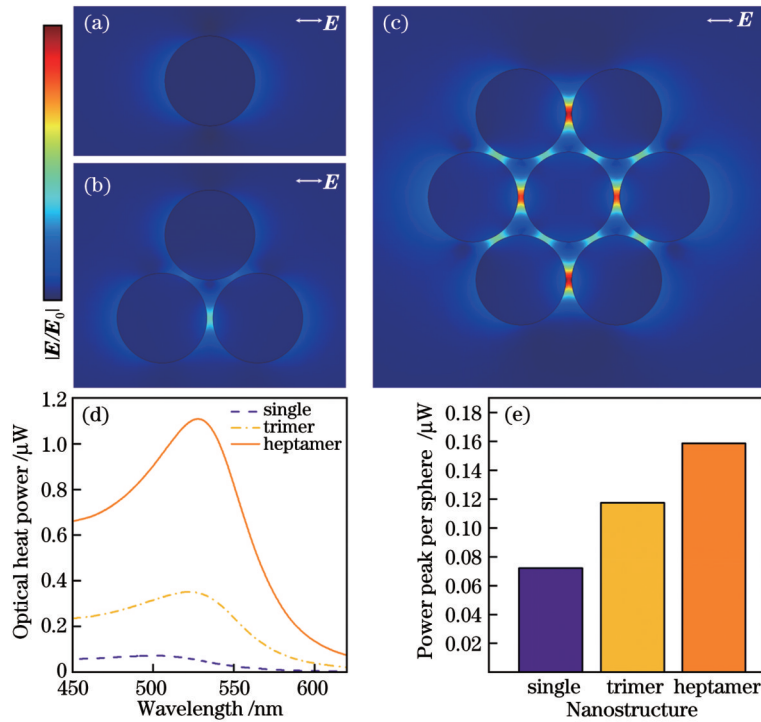


图 1 光热转换仿真。(a)~(c)孤立金纳米球、正三角形金纳米球三聚体和密排六边形金纳米球七聚体探针的局域表面等离子体共振电场增强;(d)不同耦合纳米结构纳米探针的光热功率谱仿真结果;(e)不同耦合纳米结构纳米探针中每个金纳米球的最大热功率
Fig. 1 Simulation of photothermal conversion. (a)~(c) Localized surface plasmon resonance induced electric field enhancement of nanoprobe with single gold nanosphere, equilateral triangular gold nanosphere trimer, and densely packed hexagonal gold nanosphere heptamer, respectively; (d) simulated optical heat power of nanoprobe with different coupling nanostructures; (e) simulated maximum optical heat power per nanosphere in nanoprobe with different coupling nanostructures

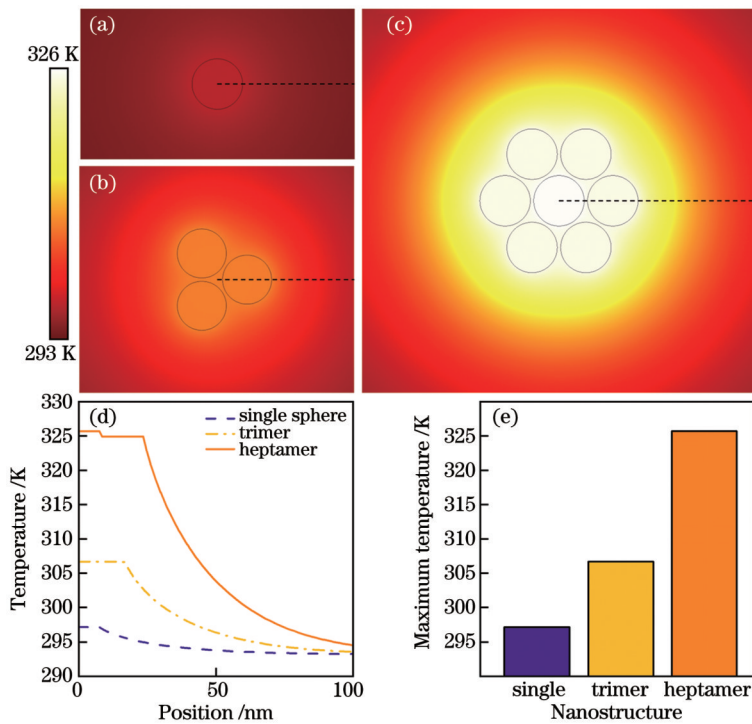


图 2 热扩散仿真。(a)~(c)孤立金纳米球、正三角形金纳米球三聚体和密排六边形金纳米球七聚体探针经电场强度为 $4 \times 10^5 \text{ V/m}$ 的激光照射 10 ns 后的定量仿真温度场;(d)虚线处的温度分布;(e)不同耦合纳米结构纳米探针经激光照射 10 ns 后的最高温度
Fig. 2 Simulation of thermal diffusion. (a)~(c) Simulated quantitative temperature fields of nanoprobe with single gold nanosphere, equilateral triangular gold nanosphere trimer, and densely packed hexagonal gold nanosphere heptamer after irradiation for 10 ns by laser with electric field intensity of $4 \times 10^5 \text{ V/m}$; (d) temperature distribution along the dotted lines in figures (a)~(c); (e) maximum temperature of nanoprobe with different coupling nanostructures after irradiation for 10 ns by laser

纳米球、正三角形金纳米球三聚体和密排六边形金纳米球七聚体探针及其周围环境的温度场。

在相同的激光照射下,与其他耦合纳米结构相比,纳米球七聚体探针表现出更显著的温度升高。出现这种现象的原因主要有两个方面:1)与其他耦合纳米结构相比,纳米球七聚体探针中每个粒子的光学吸收更强;2)小尺寸效应引起的热从纳米探针扩散到周围环境,随着纳米球数量增加,颗粒间温度场的重叠对非线性局部加热具有显著贡献。图 2(d)展示了图 2(a)~(c)中沿着黑色虚线的耦合纳米结构及其周围环境的空间温度分布。图 2(e)展示了不同耦合纳米结构下纳米探针经激光照射 10 ns 后的最高温度。从图 2(d)、(e)可以看出,在一定的激光脉冲照射下,强局域表面等离子体共振耦合的纳米探针将出现更剧烈的局部升温。

影响贵金属纳米探针电场和热耦合的一个关键因素是等离子体激元个体之间的间隙距离。如式(2)~(5)所示,电场耦合对等离子体激元个体的相对位置非

常敏感,因此纳米探针的光学吸收截面对等离子体激元个体之间的间隙具有强烈的依赖性。如图 3(a)~(c)所示,在密排六边形金纳米球七聚体探针中,当纳米球之间的间隙 d 从 2 nm 减小到 0.5 nm 时,电偶极子的集体共振和强局域表面等离子体共振诱导的电场增强更加剧烈。定量模拟了纳米球间隙 d 分别为 0.5、1、2 nm 的金纳米球七聚体探针在电场强度为 4×10^5 V/m 激光辐照下每个球体的光热功率。图 3(d)所示结果表明,随着金纳米球间隙 d 减小,金纳米球七聚体探针峰值光吸收的增加超过了 50%,吸收峰明显红移。增强的光吸收必然导致金纳米球七聚体探针温度场的变化更加强烈。如图 3(e)~(g)所示,在相同的激光辐照下,随着金纳米球间隙 d 减小,金纳米球七聚体探针及其周围环境的升温非线性增大。

为探讨纳米探针尺寸对聚集增强效应的影响,以金纳米球作为单元,选择密排六边形七聚体展开仿真实验。其中,纳米球的直径分别设定为 15、30、60 nm,

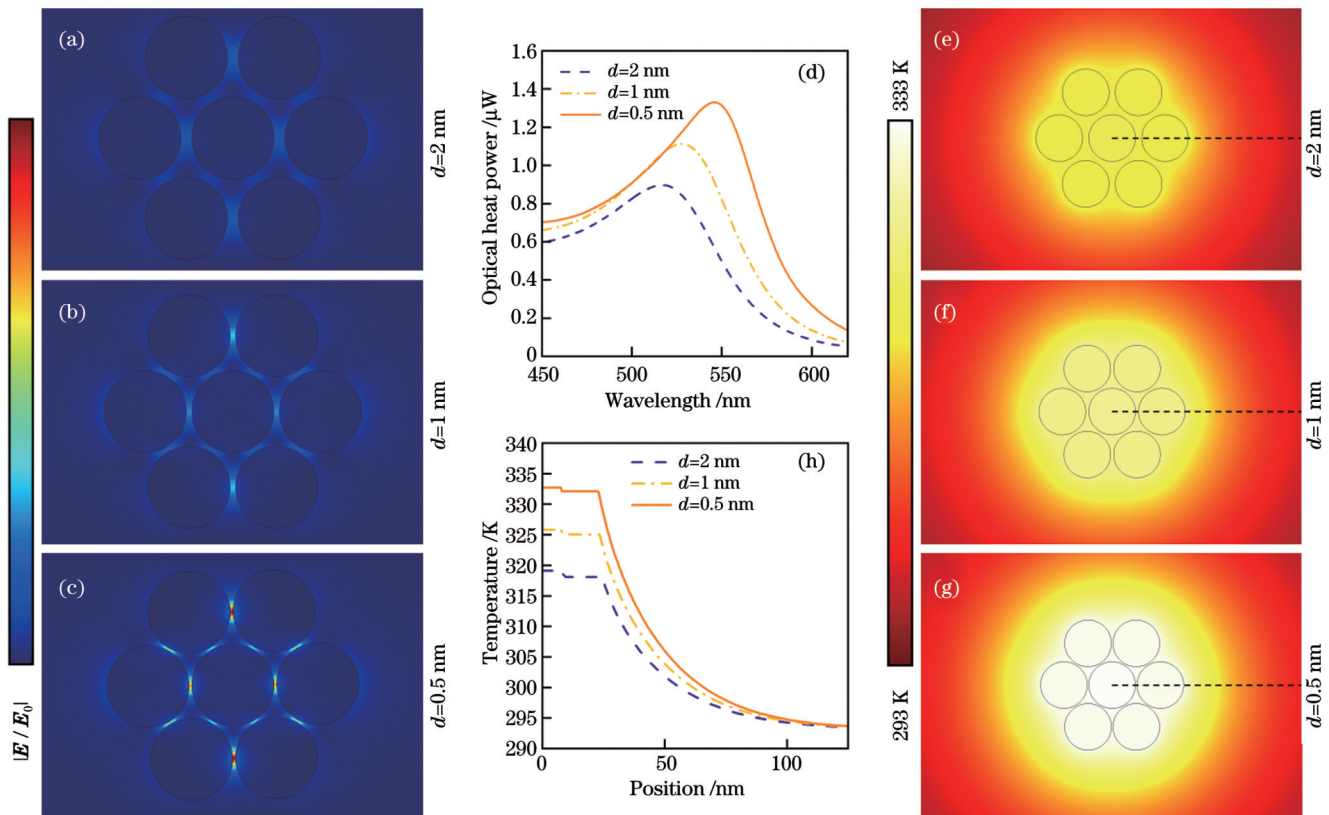


图 3 纳米球间隙 d 对纳米探针性能的影响。(a)~(c) 纳米球间隙分别为 2、1、0.5 nm 的密排六边形金纳米球七聚体探针的局域表面等离子体共振电场增强;(d) 不同纳米球间隙的密排六边形金纳米球七聚体探针的光热功率谱仿真结果;(e)~(g) 不同纳米球间隙的密排六边形金纳米球七聚体探针经电场强度为 4×10^5 V/m 的激光照射 10 ns 后的定量仿真温度场;(h) 虚线处的温度分布

Fig. 3 Influence of nanosphere-nanosphere gap (d) on nanoprobe performance. (a)–(c) Localized surface plasmon resonance induced electric field enhancement of gold nanosphere heptamer probe with nanosphere-nanosphere gap distance of 2, 1, and 0.5 nm; (d) simulated optical heat power of gold nanosphere heptamer probe with different gaps; (e)–(g) simulated quantitative temperature fields of gold nanosphere heptamer probe with different gaps after irradiation for 10 ns by a laser with electric field intensity of 4×10^5 V/m; (h) temperature distribution along the dotted lines in figures (e)–(g)

纳米球之间的间距保持定值(1 nm)。如图 4(a)~(c)所示,当用电场强度为 4×10^5 V/m 的激光脉冲照射时,随着单个纳米球直径增大,电磁场略有增强,整体的光热功率大大提高,同时吸收峰位置出现红移。为了排除增大单球直径导致纳米探针本身质量和体积增加产生的影响,本文计算了单位体积纳米金材料贡献的光热功率。计算结果表明,光热转换效率与单球直径并非一直成正相关关系。如图 4(g)所示,当直径

过大时,尽管整体的光热功率仍然有所提升,但单位体积的光热功率明显降低。图 4(d)~(f)展示了不同单球直径的纳米探针经激光照射 10 ns 后的温度场,图 4(h)为图 4(d)~(f)中虚线处的温度分布。结果显示,适当增大单球直径可以有效提高单位纳米材料的光热转换效率,并获得更好的温升效果,但单球直径过大时热源能量会出现下降,温升效果并不理想。

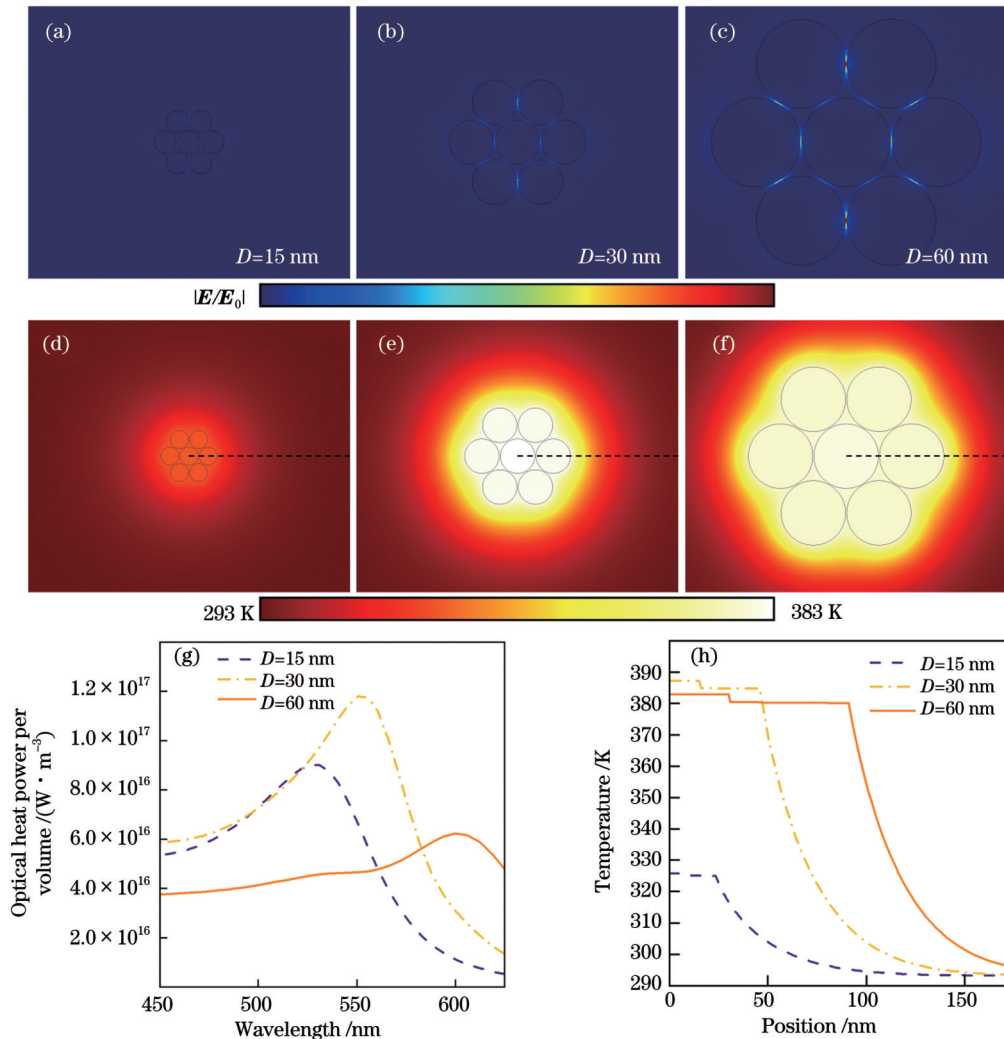


图 4 单球直径对纳米探针性能的影响。(a)~(c)单球直径分别为 15、30、60 nm 的金纳米球七聚体探针的局域表面等离子体共振电场增强;(d)~(f)不同单球直径的金纳米球七聚体探针经电场强度为 4×10^5 V/m 的激光照射 10 ns 后的定量仿真温度场;(g)不同单球直径的金纳米球七聚体探针的单位体积光热功率谱仿真结果;(h)虚线处的温度分布

Fig. 4 Influence of single-sphere diameter on nanoprobe performance. (a)–(c) Localized surface plasmon resonance induced electric field enhancement of gold nanosphere heptamer probe with single-sphere diameter of 15, 30, and 60 nm; (d)–(f) simulated quantitative temperature fields of gold nanosphere heptamer probe with different single-diameter after irradiation for 10 ns by a laser with electric field intensity of 4×10^5 V/m; (g) simulated optical heat power per volume of gold nanosphere heptamer probe with different single-sphere diameters; (h) temperature distribution along the dotted lines in figures (d)–(f)

构成单元的形状也是影响局域表面等离子体共振效应的重要因素之一。为此,本文尝试在仿真中使用不同形状的纳米颗粒(即球形、六棱柱与立方体)来构成纳米探针。为了使它们具有可比性,球形单元的直径、六棱柱底面的内接圆直径、六棱柱的高

以及立方体的边长均为 15 nm,纳米探针的组成方式如图 5(a)~(c)所示,颗粒单元间的最小间隙均为 1 nm。三种不同形状颗粒构成的探针均表现出了比较强烈的电场耦合。不同形状颗粒构成的探针的体积具有一定差异,图 5(g)展示了各形状纳米颗粒构

成的纳米探针的单位体积光热功率,可见:与纳米球相比,另外两种形状的纳米颗粒组成的纳米探针具有更高的光热转换效率。这主要是由于它们特殊的形状可以使颗粒之间具有更紧密的几何关系,从而

获得了更好的耦合效果。图 5(d)~(f)展示了不同形状纳米颗粒构成的纳米探针在激光照射 10 ns 后的温度场。图 5(h)为图(d)~(f)中虚线处的温度分布。

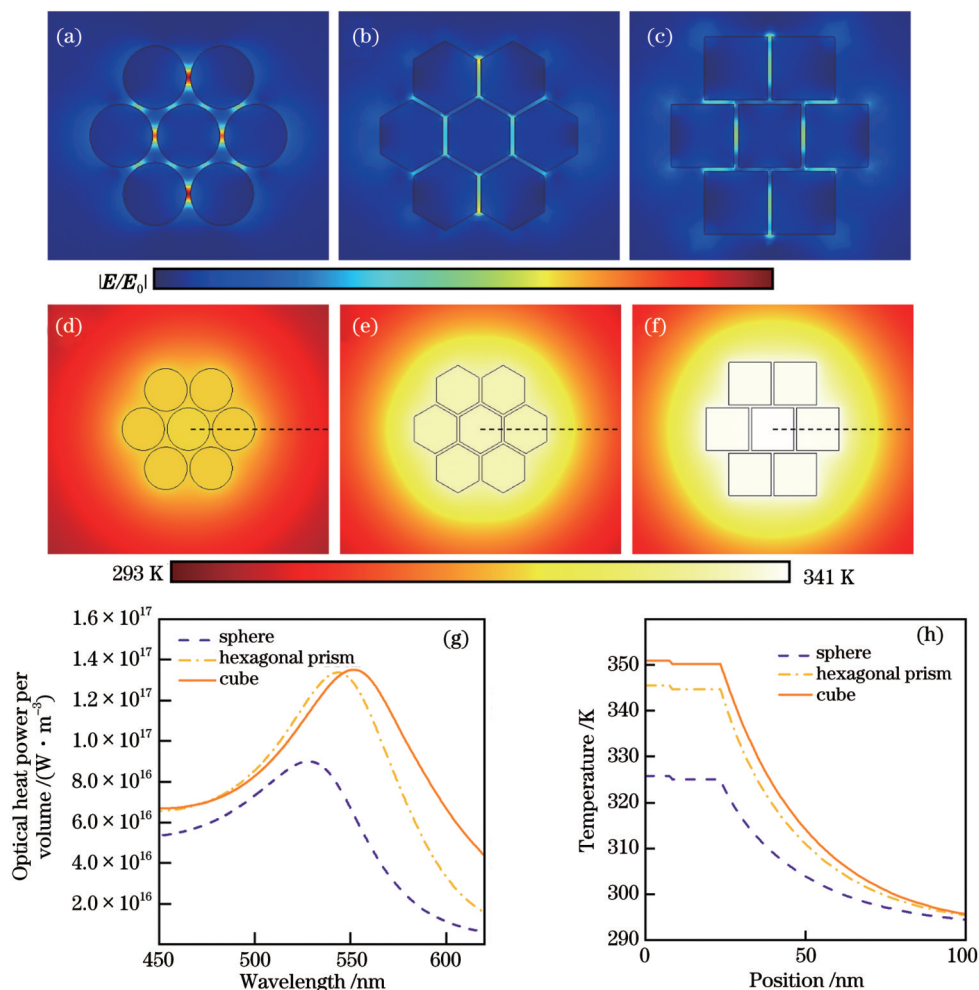


图 5 颗粒形状对纳米探针性能的影响。(a)~(c)颗粒形状分别为球形、六棱柱、立方体的金纳米七聚体探针的局域表面等离子体共振电场增强;(d)~(f)不同形状颗粒构成的金纳米七聚体探针经电场强度为 4×10^5 V/m 的激光照射 10 ns 后的定量仿真温度场;(g)不同形状颗粒构成的金纳米七聚体探针的单位体积光热功率谱仿真结果;(h)虚线处的温度分布

Fig. 5 Influence of particle shape on nanoprobe performance. (a)–(c) Localized surface plasmon resonance induced electric field enhancement of gold nano heptamers probe with spherical, hexagonal prismatic and cube particles; (d)–(f) simulated quantitative temperature fields of gold nano heptamers probe with different shapes of particles after irradiation for 10 ns by a laser with electric field intensity of 4×10^5 V/m; (g) simulated optical heat power per volume of gold nano heptamers probe with different shapes of particles; (h) temperature distribution along the dotted lines in figures (d)–(f)

在颗粒的大小、形状、数量完全相同的情况下,组装纳米探针的纳米颗粒的排列方式也是影响纳米探针性能的重要因素。在仿真实验中,本文将 7 个直径为 15 nm 的金纳米球分别以密排六边形七聚体、环形和长链形组装成纳米探针。需要说明的是,长链的排列方向与入射光的电场偏振方向平行,如图 6(a)~(c)所示。图 6(d)展示了不同排列方式下纳米探针的光热功率谱,图 6(e)~(g)展示了不同排列方式下纳米探针经激光照射 10 ns 后的温度场,图 6(h)为图(e)~(g)中虚线处的温度分布。相比于密排六边形七聚体,以环形组装的探针的光热功率略微下降。这是由于颗粒间

松散的几何关系使得耦合劣化,同时,环形排列使得热源分布更分散,所造成的温升也弱于七聚体。平行于电场偏振方向的长链形纳米组合体因具有更紧密的耦合关系而具有更高的光热功率,因此,金纳米球以长链形组装成的纳米探针具有更好的温升效果。

在设计纳米探针时,材料的选择是必须考虑的一个问题。除黄金外,铂金等其他贵金属也可以作为纳米探针材料。在仿真实验中,本文比较了直径为 15 nm 的铂纳米球在组成七聚体纳米探针前后的光热转化能力。图 7(a)、(b)分别展示了在电场强度为 4×10^5 V/m 的激光照射下单个铂纳米球和组装成的七聚体的电场

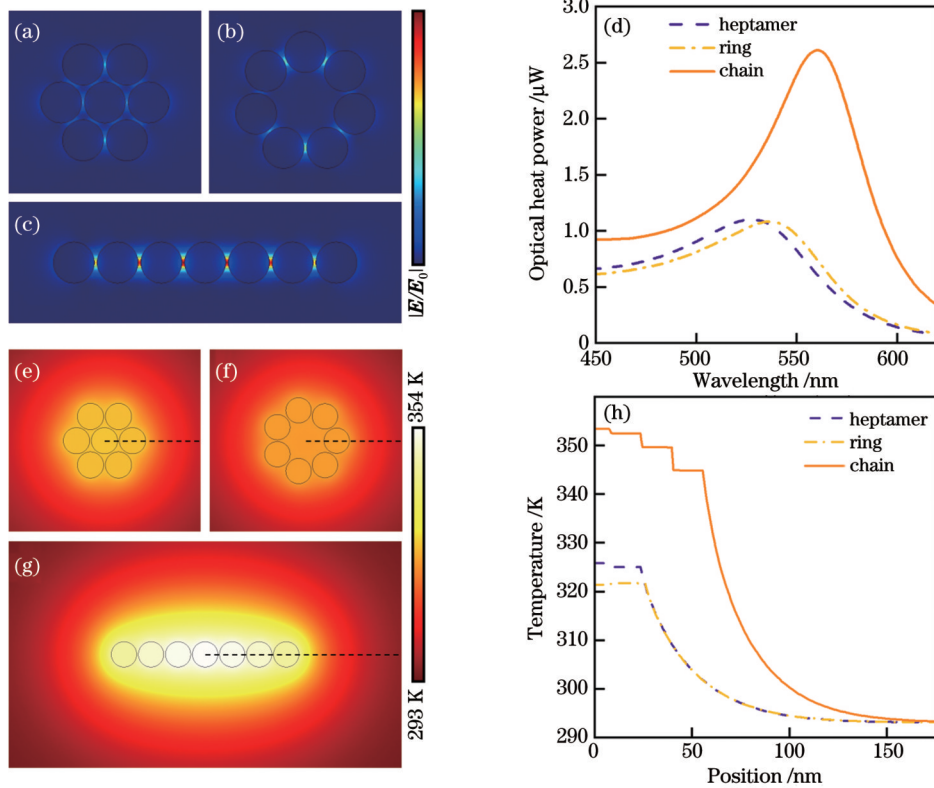


图 6 排列方式对纳米探针性能的影响。(a)~(c)纳米颗粒以密排六边形七聚体、环形和长链组成的纳米探针的局域表面等离子体共振电场增强;(d)不同排列方式下纳米探针的光热功率谱仿真结果;(e)~(g)不同排列方式下纳米探针经电场强度为 $4 \times 10^5 \text{ V/m}$ 的激光照射 10 ns 后的定量仿真温度场;(h)虚线处的温度分布

Fig. 6 Influence of permutation mode on nanoprobe performance. (a)–(c) Localized surface plasmon resonance induced electric field enhancement of nanoprobe constituted by nanoparticles with densely packed hexagonal heptamer, ring shape, and long chain; (d) simulated optical heat power of nanoprobe with different permutation modes; (e)–(g) simulated quantitative temperature fields of gold nanoprobe with different permutation modes after irradiation for 10 ns by a laser with electric field intensity of $4 \times 10^5 \text{ V/m}$; (h) temperature distribution along the dotted lines in figures (e)–(g)

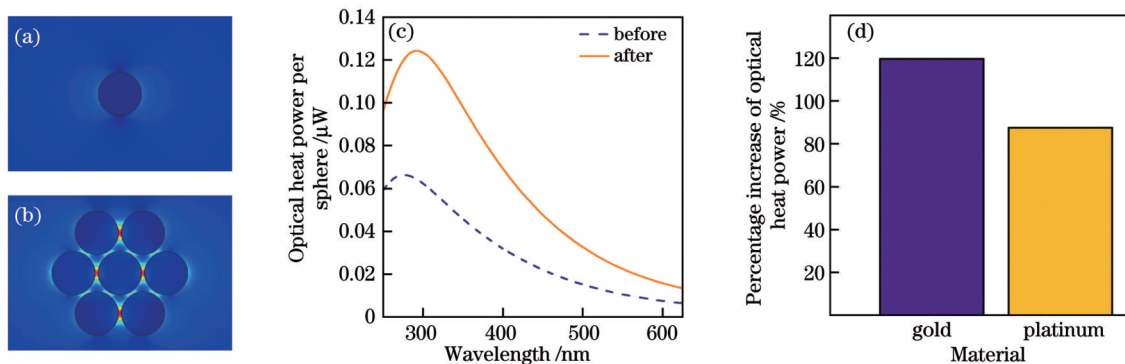


图 7 铂纳米球的聚集增强。(a)铂纳米球的电场分布;(b)铂纳米球聚集为七聚体后的电场耦合增强;(c)铂纳米球聚集为七聚体后每个纳米球的光热功率谱仿真结果;(d)金纳米球与铂纳米球聚集为七聚体后每个纳米球光热功率提升百分比

Fig. 7 Aggregation enhancement of platinum nanospheres. (a) Electric field distribution of platinum nanosphere; (b) electric field enhancement for platinum nanospheres after aggregation into heptamer; (c) simulated optical heat power per platinum nanospheres before and after aggregation into heptamer; (d) percentage increase of optical heat power per gold or platinum nanosphere after aggregation into heptamer

分布,可以观察到与金纳米球十分类似的电场耦合增强现象。图 7(c)显示,当铂纳米球组装成为七聚体后,每个纳米球的光热功率提升超过了 80%(与组装前相比)。图 7(d)展示了上述条件下金和铂的纳米球在组装成七聚体后光热功率的提升百分比,相较之下,

铂材质的纳米探针的非线性聚集增强效应稍差。该组结果说明,以等离子激元共振耦合为机制的光热非线性增强普遍适用于多种贵金属纳米材料。同时也可以发现,由于材料本身的物理性质有所区别,材料物理性质对吸收峰位置的影响远远高于其他因素(铂纳米

球及其聚合物的共振吸收峰在紫外波段),因此使用不同的材料时,应特别注意与其配合使用的激光光源波长的选择。

3 分析与讨论

纳米颗粒的自组装一直是科学和技术领域的热门话题。在理论指导下合理设计和构建纳米组件可以有效促进其在光热治疗及其他领域的应用。本文构建了一定纳米耦合结构的贵金属纳米探针,证明了聚集诱导的非线性增强的光热效应。综合分析各种因素的影响后发现,局域表面等离子体共振耦合增强的本质是外电场将纳米单元激发为电偶极子后,偶极子所激发的电场对周围其他偶极子的作用。因此,设计高光热转换效率的关键在于尽量使偶极子处于其他偶极子所激发电场的更强处。仿真实验有力地证明了合理设计颗粒的聚集程度、间隙、尺寸、形状和排列方式是实现目标的有效途径。虽然本文仅显示了二维耦合纳米探针,但该策略可以容易地扩展到具有更高耦合效率的三维耦合纳米组件上,并且可以预期非线性增强的光热效应。不过,在实际生物应用中还应考虑贵金属纳米探针的结构稳定性。

4 结论

本文定量模拟了局域表面等离子体共振耦合贵金属纳米探针的非线性增强光热效应。与孤立纳米颗粒相比,更多的纳米粒子在空间聚集并组成一定的纳米耦合结构后,纳米颗粒之间的强光学和热耦合作用可以实现每个颗粒加权光学吸收的几倍增强以及相应的热场增强。本文定量讨论了非线性光热增强效应对颗粒聚集数量的依赖性,讨论了颗粒间隙、尺寸、形状、排列方式等对纳米探针光热转换效率的影响,证实了以等离子体共振耦合为机制的光热非线性增强在多种贵金属纳米材料中具有广泛的适用性。基于有限元分析技术展开模拟仿真研究,仿真结果很好地印证了理论分析的正确性。本工作为合理设计具有更高光吸收率与光热转换效率的贵金属纳米探针提供了借鉴。

参 考 文 献

- [1] Chen Q, Wang C, Zhan Z X, et al. Near-infrared dye bound albumin with separated imaging and therapy wavelength channels for imaging-guided photothermal therapy[J]. *Biomaterials*, 2014, 35(28): 8206-8214.
- [2] Li W T, Sun X L, Wang Y, et al. *In vivo* quantitative photoacoustic microscopy of gold nanostar kinetics in mouse organs[J]. *Biomedical Optics Express*, 2014, 5(8): 2679-2685.
- [3] Peng Y, Liu Y, Lu X L, et al. Ag-hybridized plasmonic A-triangular nanoplates: highly sensitive photoacoustic/Raman evaluation and improved antibacterial/photothermal combination therapy[J]. *Journal of Materials Chemistry B*, 2018, 6(18): 2813-2820.
- [4] Xu J W, Cheng X J, Chen F X, et al. Fabrication of multifunctional polydopamine-coated gold nanobones for PA/CT imaging and enhanced synergistic chemo-photothermal therapy[J]. *Journal of Materials Science & Technology*, 2021, 63: 97-105.
- [5] Li Y, Liu G H, Ma J Y, et al. Chemotherapeutic drug-photothermal agent co-self-assembling nanoparticles for near-infrared fluorescence and photoacoustic dual-modal imaging-guided chemo-photothermal synergistic therapy[J]. *Journal of Controlled Release*, 2017, 258: 95-107.
- [6] Clavero C. Plasmon-induced hot-electron generation at nanoparticle/metal-oxide interfaces for photovoltaic and photocatalytic devices[J]. *Nature Photonics*, 2014, 8(2): 95-103.
- [7] Ng S M, Koneswaran M, Narayanaswamy R. A review on fluorescent inorganic nanoparticles for optical sensing applications[J]. *RSC Advances*, 2016, 6(26): 21624-21661.
- [8] Wang S S, Chen R H, Yu Q, et al. Near-infrared plasmon-boostered heat/oxygen enrichment for reversing rheumatoid arthritis with metal/semiconductor composites[J]. *ACS Applied Materials & Interfaces*, 2020, 12(41): 45796-45806.
- [9] 徐娅, 边捷, 张伟华. 局域表面等离子体共振耦合纳米光学传感器的原理与进展[J]. *激光与光电子学进展*, 2019, 56(20): 202407.
- [10] Xu Y, Bian J, Zhang W H. Principles and processes of nanometric localized-surface-plasmonic optical sensors[J]. *Laser & Optoelectronics Progress*, 2019, 56(20): 202407.
- [11] 陈泓先, 孙宁, 张洁. 泡沫镍耦合金纳米结构增强拉曼散射[J]. *光学学报*, 2022, 42(5): 0524001.
- [12] Chen H X, Sun N, Zhang J. Nickel foam coupled gold nanostructures enhanced Raman scattering[J]. *Acta Optica Sinica*, 2022, 42(5): 0524001.
- [13] 黄向民, 施慧, 赵航, 等. 基于光热效应的纳米塑料捕获和SERS检测[J]. *光学学报*, 2022, 42(16): 1624001.
- [14] Huang X M, Shi H, Zhao H, et al. Capture and SERS detection of nano plastics based on photothermal effect[J]. *Acta Optica Sinica*, 2022, 42(16): 1624001.
- [15] Yang X, Yang M X, Pang B, et al. Gold nanomaterials at work in biomedicine[J]. *Chemical Reviews*, 2015, 115(19): 10410-10488.
- [16] Hutter E, Fendler J H. Exploitation of localized surface plasmon resonance[J]. *Advanced Materials*, 2004, 16(19): 1685-1706.
- [17] Fan J A, Wu C, Bao K, et al. Self-assembled plasmonic nanoparticle clusters[J]. *Science*, 2010, 328(5982): 1135-1138.
- [18] Zheng M B, Yue C X, Ma Y F, et al. Single-step assembly of DOX/ICG loaded lipid: polymer nanoparticles for highly effective chemo-photothermal combination therapy[J]. *ACS Nano*, 2013, 7(3): 2056-2067.
- [19] Rechberger W, Hohenau A, Leitner A, et al. Optical properties of two interacting gold nanoparticles[J]. *Optics Communications*, 2003, 220(1/2/3): 137-141.
- [20] Huang P, Lin J, Li W W, et al. Biodegradable gold nanovesicles with an ultrastrong plasmonic coupling effect for photoacoustic imaging and photothermal therapy[J]. *Angewandte Chemie (International Ed. in English)*, 2013, 52(52): 13958-13964.
- [21] Dey P, Tabish T A, Mosca S, et al. Plasmonic nanoassemblies: tentacles beat satellites for boosting broadband NIR plasmon coupling providing a novel candidate for SERS and photothermal therapy[J]. *Small*, 2020, 16(10): 1906780.
- [22] Liu Y P, Zhang X W, Luo L Y, et al. Gold-nanobranched-shell based drug vehicles with ultrahigh photothermal efficiency for chemo-photothermal therapy[J]. *Nanomedicine: Nanotechnology, Biology and Medicine*, 2019, 18: 303-314.
- [23] Li X M, Yu L C, Zhang C N, et al. Tumor acid microenvironment-activated self-targeting & splitting gold nanoassembly for tumor chemo-radiotherapy[J]. *Bioactive Materials*, 2022, 7: 377-388.
- [24] Draine B T, Flatau P J. Discrete-dipole approximation for scattering calculations[J]. *Journal of the Optical Society of America A*, 1994, 11(4): 1491-1499.
- [25] Gunnarsson L, Rindzevicius T, Prikulis J, et al. Confined plasmons in nanofabricated single silver particle pairs: experimental observations of strong interparticle interactions[J]. *The Journal of Physical Chemistry B*, 2005, 109(3): 1079-1087.

Quantitative Simulation of Nonlinear Enhanced Photothermal Effect Induced by Aggregation of Noble-Metal Nanoprobe

Zhang Qirui^{1,2}, Shi Yujiao^{1,2*}

¹MOE Key Laboratory of Laser Life Science & Institute of Laser Life Science, College of Biophotonics, South China Normal University, Guangzhou 510631, Guangdong, China;

²Guangdong Provincial Key Laboratory of Laser Life Science, College of Biophotonics, South China Normal University, Guangzhou 510631, Guangdong, China

Abstract

Objective Photothermal therapy is a tumor treatment method that converts optical energy into thermal energy, kills tumor cells via local heating, and triggers biochemical processes. A necessary condition for the development of photothermal therapy is to obtain a highly efficient probe for photothermal conversion with satisfactory safety and targeting. The use of nanoprobes coupled by local surface plasmon resonance is one of the latest research and development directions in photothermal therapy. Because local surface plasmon resonance significantly depends on specific nanostructures, the position of the extinction peak is adjusted to locate in the optical window of biological tissues, and the extinction intensity is adjusted to achieve appropriate photothermal conversion efficiency, which can be theoretically achieved through the morphological design of nanoprobes. However, it remains challenging to design these nanoprobes under quantitative guidance. In this study, we systematically investigated and quantitatively analyzed the nonlinear optical field and photothermal enhancement effect produced using the local surface plasmon resonance coupling effect and their mechanisms caused by various factors. This approach provides systematic and comprehensive theoretical guidance for designing efficient plasma nanoaggregation probes.

Methods In this study, the nonlinear optical and photothermal effects induced by the aggregation of noble metal nanoprobes were quantitatively demonstrated using finite element simulations. In each simulation experiment, nanoprobes with different degrees of aggregation, gap distances, particle sizes, shapes, permutations, and materials of nanoparticles were constructed to evaluate the influence of these factors on the aggregation enhancement effect and photothermal conversion efficiency. For the degree of aggregation, isolated gold nanospheres, regular-triangular gold nanosphere trimers, and hexagonal gold nanosphere heptamers were used as examples. For the gap distance, we quantitatively simulated gold nanosphere heptamers with gap distances of 0.5, 1, and 2 nm. For the particle size, simulated gold nanosphere heptamers with spherical diameters of 15, 30, and 60 nm were used. For the particle shape, simulated gold nanoheptamers with spheres, hexagonal prisms, and cubes were used. For permutations, simulated heptamers, rings, and chains were used. Gold and platinum were compared.

Results and Discussions Self-assembly of nanoparticles has been a prominent topic in science and technology. Under the guidance of theory, the reasonable design and construction of nanocomponents can effectively promote their applications in photothermal therapy and other fields. In this study, noble metal nanoprobes with a specific nanocoupling structure were constructed to demonstrate the photothermal effect of nonlinear enhancement induced by aggregation. The essence of enhanced local surface plasmon resonance coupling is that, after the external electric field excites the nanounit into an electric dipole, the electric field excited by the dipole acts on other nearby dipoles. Therefore, the key to designing a high photothermal conversion efficiency is to make the dipole as strong as possible in an electric field excited by other dipoles. The simulation experiment demonstrated that a reasonable design of the degree of aggregation, gap distance, particle size, shape, and arrangement is adequate for achieving this goal. Although only two-dimensional coupled nanoprobes are shown, this approach can be easily extended to three-dimensional coupled nanocomponents with increased coupling efficiency, and nonlinear enhanced photothermal effects can be expected.

Conclusions We quantitatively simulated the nonlinear enhanced photothermal effect of local surface plasmon resonance-coupled noble metal nanoprobes. Instead of isolated nanoparticles, a large number of nanoparticles gather in space and form a specific nanocoupling structure. The strong optical and thermal coupling between the nanoparticles results in an enhancement of the weighted optical absorption of each particle by several times and the corresponding thermal field enhancement. The dependence of the nonlinear photothermal enhancement effect on the aggregation quantity is discussed quantitatively. Moreover, the effects of the gap distance, particle size, shape, and arrangement mode on the photothermal conversion efficiency of the nanoprobe were discussed extensively. The photothermal nonlinear enhancement mechanism based on the plasmon resonance coupling mechanism is widely applicable to various precious metal nanomaterials. Based on finite element analysis, simulations were conducted, and the simulation results reflected the theoretical discussion satisfactorily. This study paves the way for the rational design and optimization of noble metal nanoprobes with higher light absorption and photothermal conversion efficiency.

Key words bio-optics; nanoprobes; photothermal conversion; localized surface plasmon resonance; coupling effect